TRW

S/N 60024

MICROLASER ARRAY DEVELOPMENT

Final Report

Item No. 0002AD

December 23, 1994

Sponsored by

Defense Advanced Research Projects Agency

Effort/ Microlaser Array Development

ARPA Order No. 8779

Issued by DARPA/CMO under Contract # MDA972-92-C-0048

Program manager: Michael Wickham

TRW Space and Technology Group

One Space Park

Redondo Beach, California, 90278

"The views and conclusions contained in this documaent are those of the authors and should not be interpreded as representing the official policies, either expressed of implied, of the Defense Advanced Research Projects Agency or the U.S. Government."

ADVANCED RESEARCH PROJECTS AGENCY
3701 NORTH FAIRFAX DRIVE
ARLINGTON, VA 22203-1714

JAN 29 1996

MEMORANDUM FOR DTIC-OCC
ATTENTION: (CRYSTAL RILEY)

SUBJECT: Distribution Statements on Technical Documents

This is in response to your memorandum requesting a distribution statement for the document entitled "Microlaser Array Development, Final Report." All copies should carry the Distribution Statement "A" (Approved for Public Release; Distribution is Unlimited).

Debra K. Amick
Technical Information Officer

Attachments

OFFICE OF THE UNDER SECRETARY OF DEFENSE (ACQUISITION & TECHNOLOGY)
DEFENSE TECHNICAL INFORMATION CENTER
8725 JOHN J KINGMAN RD STE 0944
FT BELVOIR VA 22060-6218

IN REPLY
REFER TO

DTIC-OMI

SUBJECT: Distribution Statements on Technical Documents

TO:
ARPA/TIO
3701 NORTH FAIRFAX DRIVE
ARLINGTON, VA 22203-1714

1. Reference: DoD Directive 5230.24, Distribution Statements on Technical Documents, 18 Mar 87.

2. The Defense Technical Information Center received the enclosed report (referenced below) which is not marked in accordance with the above reference.

FINAL REPORT
23 DEC 94
MDA972-92-C-0048

3. We request the appropriate distribution statement be assigned and the report returned to DTIC within 5 working days.

4. Approved distribution statements are listed on the reverse of this letter. If you have any questions regarding these statements, call DTIC's Input Support Branch, (703) 767-9092, 9088 or 9086 (DSN use prefix 427).

FOR THE ADMINISTRATOR:

1 Encl

CRYSTAL RILEY
Chief, Input Support Branch

FL-171
Dec 95

DoD Directive 5230.24, "Distribution Statements on Technical Documents," 18 Mar 87, contains seven distribution statements, as described briefly below. Technical Documents that are sent to DTIC **must** be assigned one of the following distribution statements:

☒ **DISTRIBUTION STATEMENT A:**

APPROVED FOR PUBLIC RELEASE; DISTRIBUTION IS UNLIMITED.

☐ **DISTRIBUTION STATEMENT B:**

DISTRIBUTION AUTHORIZED TO U. S. GOVERNMENT AGENCIES ONLY; (FILL IN REASON); (DATE STATEMENT APPLIED). OTHER REQUESTS FOR THIS DOCUMENT SHALL BE REFERRED TO (INSERT CONTROLLING DoD OFFICE).

☐ **DISTRIBUTION STATEMENT C:**

DISTRIBUTION AUTHORIZED TO U. S. GOVERNMENT AGENCIES AND THEIR CONTRACTORS; (FILL IN REASON); (DATE STATEMENT APPLIED). OTHER REQUESTS FOR THIS DOCUMENT SHALL BE REFERRED TO (INSERT CONTROLLING DoD OFFICE).

☐ **DISTRIBUTION STATEMENT D:**

DISTRIBUTION AUTHORIZED TO DoD AND DoD CONTRACTORS ONLY; (FILL IN REASON); (DATE STATEMENT APPLIED). OTHER REQUESTS SHALL BE REFERRED TO (INSERT CONTROLLING DoD OFFICE).

☐ **DISTRIBUTION STATEMENT E:**

DISTRIBUTION AUTHORIZED TO DoD COMPONENTS ONLY; (FILL IN REASON); (DATE STATEMENT APPLIED). OTHER REQUESTS SHALL BE REFERRED TO (INSERT CONTROLLING DoD OFFICE).

☐ **DISTRIBUTION STATEMENT F:**

FURTHER DISSEMINATION ONLY AS DIRECTED BY (INSERT CONTROLLING DoD OFFICE AND DATE), OR HIGHER DoD AUTHORITY.

☐ **DISTRIBUTION STATEMENT X:**

DISTRIBUTION AUTHORIZED TO U. S. GOVERNMENT AGENCIES AND PRIVATE INDIVIDUALS OR ENTERPRISES ELIGIBLE TO OBTAIN EXPORT-CONTROLLED TECHNICAL DATA IN ACCORDANCE WITH DoD DIRECTIVE 5230.25 (DATE STATEMENT APPLIED). CONTROLLING DoD OFFICE IS (INSERT).

Unlimited
(Reason)

ARPA
(Assigning Office)

Debra K. Amick
Debra K. Amick
Technical Information Officer
(OASB/TIO)
Advanced Research Projects Agency
3701 North Fairfax Drive
Arlington, VA 22203-1714
(703) 696-2301

OASB / TIO
(Controlling DoD Office Name)
ARPA/TIO
3701 North Fairfax Drive
Arlington, VA 22203-1714
(Controlling DoD Office Address (City/State/Zip)

JAN 29 1996
(Date Statement Assigned)

37424

REPORT DOCUMENTATION PAGE

Form Approved
OMB No. 0704-0188

1. AGENCY USE ONLY (Leave blank)	2. REPORT DATE	3. REPORT TYPE AND DATES COVERED
	December 23, 1994	Final Report 07/08/92 - 11/15/93

4. TITLE AND SUBTITLE
Microlaser Array Development

5. FUNDING NUMBERS
Contract #MDA972-92-C-0048

6. AUTHOR(S)
Michael Wickham, Phil Hayashida

7. PERFORMING ORGANIZATION NAME(S) AND ADDRESS(ES)
TRW Space & Technology Group
One Space Park
Redondo Beach, CA. 90278

8. PERFORMING ORGANIZATION REPORT NUMBER

9. SPONSORING/MONITORING AGENCY NAME(S) AND ADDRESS(ES)
Advanced Research Project Agency

10. SPONSORING/MONITORING AGENCY REPORT NUMBER

11. SUPPLEMENTARY NOTES

12a. DISTRIBUTION/AVAILABILITY STATEMENT

DISTRIBUTION STATEMENT A
Approved for public release
Distribution Unlimited

DTIC QUALITY INSPECTED 5

12b. DISTRIBUTION CODE

13. ABSTRACT (Maximum 200 words)

This report describes the design, construction and characterization of a 2 dimensional micro laser array. The micro laser array consists of a monolithic pump array, microlenses, and a solid state gain module. Passive q-switching on a single element was also demonstrated on this program. The array produced 0.35 Watts of average power with an optical efficiency of 5.8%. 70 elements out of the 108 total elements were laseing and the best elements were lasing at 2 μJ energy per pulse and with 12% optical efficiency. The diode array pump was a TRW built, high power surface emitting array, HPSEA, device cooled by a TRW built micro channel heat exchanger. The gain material was 400 μ thick Nd:YVO_4 and the output wavelength was 1.064 μ. The far field divergence of the entire array was 10.4 mrad and 3.5 mrad for a single element. Each of the elements in the array operated single longitudinal and single transverse mode. The frequency variation over the entire array was 43 GHz and was due to individual variations in cavity lengths.

14. SUBJECT TERMS	15. NUMBER OF PAGES
	41
	16. PRICE CODE

17. SECURITY CLASSIFICATION OF REPORT	18. SECURITY CLASSIFICATION OF THIS PAGE	19. SECURITY CLASSIFICATION OF ABSTRACT	20. LIMITATION OF ABSTRACT
Unclassified	Unclassified	Unclassified	

Table of Contents

1. INTRODUCTION

The number of applications for microlaser arrays is increasing. Potential government applications include: laser radar, missile guidance, remote sensing, target and terrain illuminators/mappers for aircraft, and identification friend or foe (IFF). In an IFF scenario, when a detector array element on a ground vehicle is designated by friendly aircraft, a corresponding microlaser array element transmits a recognition signal to that aircraft.

Affordable, compact laser-arrays (microlaser arrays) are critical to enable these applications. Optimally, microlaser arrays are miniaturized lasers which can be produced in large volumes using standard chip manufacturing techniques. They are small in size, operate pulsed or continuous wave (CW), can be low cost, and potentially scalable in modular fashion. In addition the microlaser array must be efficient to avoid thermal limitations and achieve high powers.

The purpose of this program was to develop a scalable integrated microlaser array consisting of a monolithic pump array, microlenses, and a solid state gain module. A second goal was to demonstrate passive q-switching. The TRW 2-D microarray concept employed is illustrated in Figure 1.1.

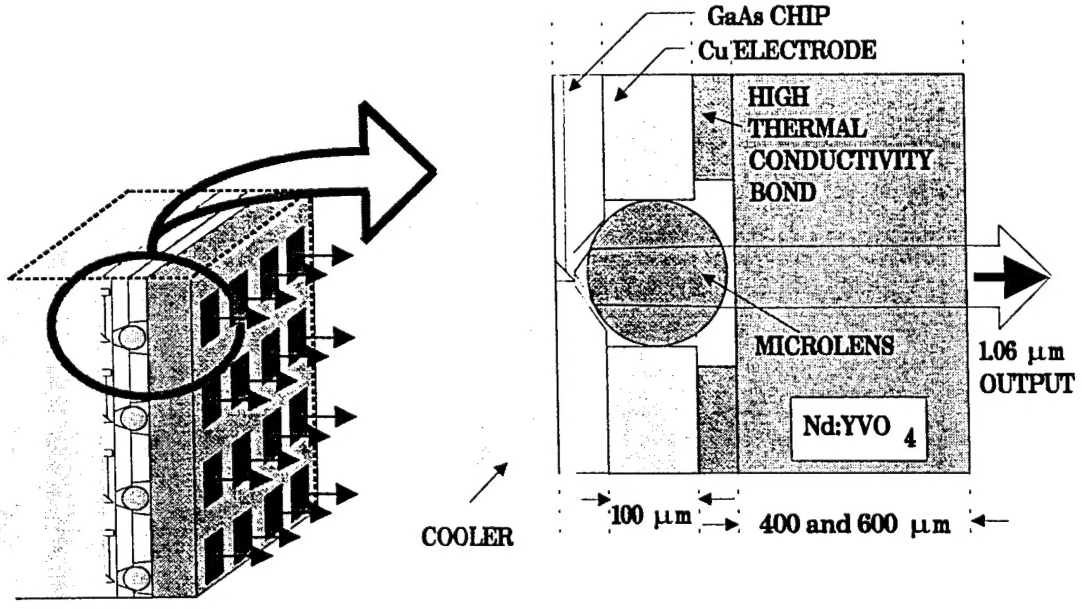

Figure 1.1 Monolithic Microlaser Array Geometry

The program used a number of unique technologies already developed at TRW. These technologies included: 2-D monolithic surface-emitting diode arrays, microchannel heat exchangers, diode-pumped solid state slab lasers, and compact solid state Q-switch material.

The TRW approach uses:

* Batch processing and assembly techniques, compatible with low cost commercial manufacturing, to fabricate the 2-D pumps.
* A planar pump geometry providing flat surfaces for easy mounting of both the heat sink and the solid state slab, resulting in a planar microarray that is both solid and compact.
* Integrated shaped-fiber microlenses which collimate the diode laser output for efficient pumping of the solid state material.
* Microchannel heat exchangers with a short thermal path (SEA mounted junction down) to the "hot" SEA active region, allowing the 2-D monolithic pump to be operated at high duty cycles to high powers.

Pumped at 809 nm, the chosen solid state material, Nd:YVO_4, has a high absorption crossection which allows us to use thin, light weight slabs. The high gain and emission cross-section (low saturation fluence) of Nd:YVO_4 makes it ideal for Q-switched operation.

Figure 1.2 shows the microlaser array (left side) and a few of the envisioned applications (right side) that are compatible with the TRW design. The middle picture shows integrated Q-switching and frequency doubling providing high peak powers.

The first application involves phase locking of microlaser arrays in an external cavity configuration. It is based on the Talbot diffractive coupling concept for an array of coherent periodic sources(1). The application includes: the microlaser array evolved from this program, aperture filling microlenses, a reflector plate (sides are reflective) which makes a finite 2-D array appear infinite, a liquid crystal phase plate to correct for piston error, and the external cavity mirror. Single longitudinal mode operation from all sources vastly improves locking in this type of an external cavity configuration.

The second application shown is a scaled-up version of the microlaser arrays. Since the arrays are modular, many such modules can be connected electrically in series to form large systems.

The third application integrates an optical parametric oscillator (OPO) for multi-wavelength operation.

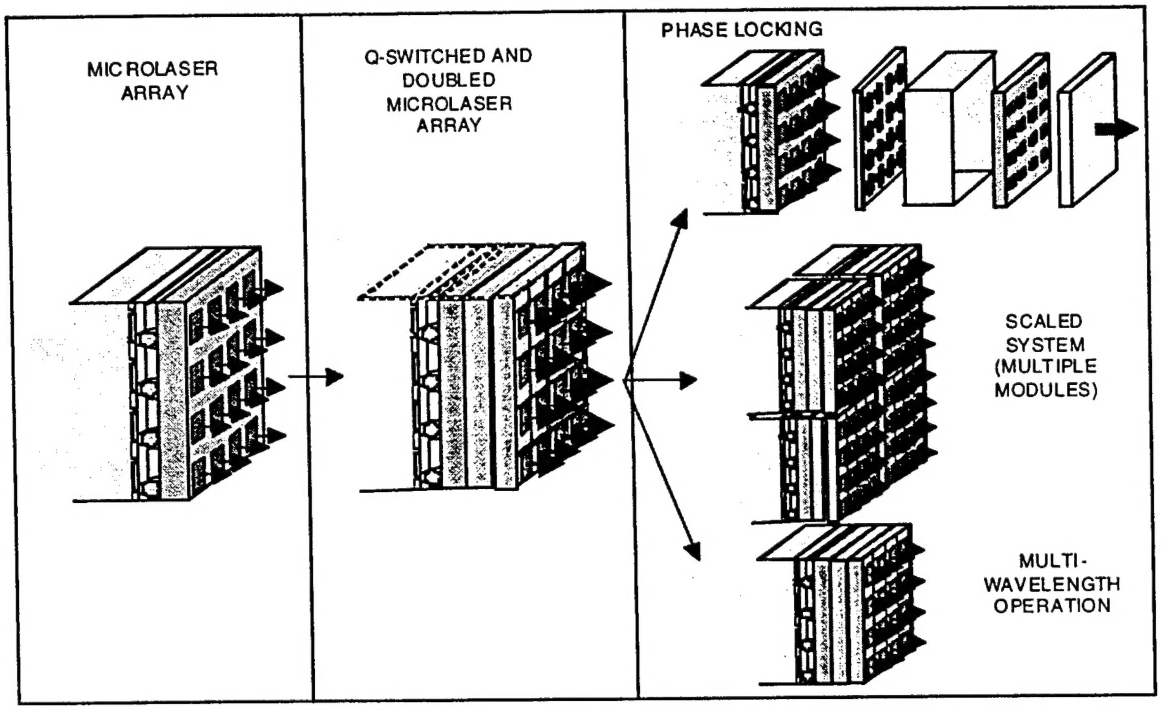

Figure 1.2 Microlaser Array (left), Microlaser Array for High Peak Powers (center), Microlaser Applications (right)

Figure 1.3 shows the microlaser design requirements and the performance demonstrated in this program.

DESIGN REQUIREMENTS		DEMONSTRATED RESULTS
MICROLASER ARRAY	TWO DIMENSIONAL (2-D), > 100 ELEMENTS	70 elements
	DUTY CYCLE = 5% (10% GOAL)	35%
	AVERAGE POWER 250 mW (400 mW GOAL)	350 mW
	OPTICAL EFFICIENCY = 16% (20% GOAL)	5.8%
	SINGLE LONGITUDINAL MODE OPERATION	YES
	Q-SWITCHED OPERATION	SINGLE MICROLASER
PUMP ARRAY	TWO-DIMENSIONAL MONOLITHIC	YES
	AREA = > 0.5 cm^2	YES
	PEAK POWER = 50 W	17.4 W
	WAVELENGTH = 809 $\pm$ 2.5 nm	YES
	PULSE WIDTH > 100 ms	YES

Figure 1.3 Design Requirements and Results on this Program

The key diode technologies, such as CW monolithic surface emitting arrays, and microchannel heat exchangers were developed on the "High Power Surface Emitting Array Program", sponsored by Wright Laboratory (WL). Some results include peak output power densities of > 100 W/cm^2 at 35% duty cycles, high power conversion efficiencies (22%), and full width emission spectra of < 4 nm for arrays, as well as 50 W/cm^2 under CW operation for arrays packaged for that purpose. The arrays were mounted on silicon microchannel heat exchangers, which had a thermal resistance per unit area of 0.0324 ^oC cm^2/W, and which were used to remove up to 550 W/cm^2 of excess heat generated by the arrays. These are the highest optical powers reported for monolithic arrays emitting at 808 nm under high duty cycle and CW operation, as well as the best reported microchannel cooling performance.

2. MICROLASER DESIGN

2.1 Baseline Design

The baseline design for the program is summarized in tables below (a-d). It includes the overall system, and the components (solid state slab, Q-switch material, and diode array pump).

ENERGY STORED	16mJ/ELEMENT
SPOT DIAMETER	50-100 mm
ROUND TRIP SMALL SIGNAL GAIN	1.2 - 2.5
ENERGY EXTRACTED	8 mJ/ELEMENT
LONGITUDINAL MODE SPECTRUM	SINGLE LONGITUDINAL MODE
OPTICAL EFFICIENCY	20%
PEAK ARRAY POWER	8 W
DUTY CYCLE	10%
PULSE WIDTH	100 us
REPETITION RATE	1 kHz

(a) Predicted Microlaser Array Performance

MATERIAL	Nd:YVO_4
EMISSION WAVELENGTH	1.064 mm
DOPING LEVEL	1.1%
FLUORESCENCE LIFETIME	90 μs
MATERIAL THICKNESS	400 AND 600 mm

(b) Laser Medium

MATERIAL	Cr^{4+}:YAG
PULSE DURATION	2 ns (INDIVIDUAL LASERS)

(c) Q-Switch

NUMBER OF ELEMENTS	108 (9X12 ARRAY)
ARRAY AREA	0.5 cm^2
EMISSION WAVELENGTH	809 $\pm$ 2.5 nm
DIODE POWER	500 mW/ELEMENT
DIODE PULSE LENGTH	100 us
DUTY CYCLE	5% (500 Hz); 10% (1KHz) GOAL

(d) Pump Array

2.2 Design Trades

The TRW system design trades are broken down at the laser diode and solid state subsystem level and are addressed in the next two sections.

2.2.1 Diode Arrays

The design logic that supports our selection of surface emitting arrays (SEAs) is summarized here. The key requirements on microlaser array pumps are low cost manufacturing, compact packaging, and efficient heat removal.

Because of batch wafer processing, and self-aligned packaging and assembly, the monolithic surface emitting fabrication involves a small number of assembly steps and results in significant cost savings for large area pumps versus the rack and stack (R&S) approach. The Rack and Stack approach requires a large number of assembly steps in mounting the individual laser bars.

Self-alignment of shaped fiber collimating optics (microlenses) in lithographically defined grooves (~ 1 μm accuracy) is a key advantage over the R&S approach where arrays lack symmetry in device positioning, and devices are difficult to align to microlenses. Compact packaging clearly favors the monolithic surface emitting architecture.

Due to a lower loss design, and greater optical power density, 45° micromirrors are preferred over vertical cavity surface emitters for outcoupling of the laser radiation in monolithic pumps. The short gain lengths in a vertical emitter necessitate high reflectivity output mirrors which lower efficiency relative to the horizontal design. A horizontal structure can dissipate heat through a shorter path and a larger area than the vertical design, and does not have the higher thermal impedance material (of the mirrors) in the thermal path. Thus both efficiency and thermal considerations favor our choice of a horizontal broad-area stripe-geometry, graded-index separate confinement heterostructure (GRIN-SCH) and single quantum well (SQW) laser diode design.

In a direct comparison with R&S pumping, the monolithic approach offers a thermal advantage for large duty cycle and CW applications. This is largely due to the very short thermal path to the heat sink in the monolithic geometry. In addition, the planar aspect of the monolithic design makes it well suited to integration with efficient microchannel heat exchangers. Furthermore, the microlaser crystal can be mounted directly on the diode array and be cooled through the substrate, greatly simplifying packaging.

The thermal performance of a monolithic SEA array out performs R&S configurations. We compared the thermal performance of monolithic IPSEAs with that of the competing stacked bar technologies using "DTHERM", which is a one dimensional transient conduction model based on finite differences. The input to the code is the thickness and thermal properties of multiple layers of different materials, and the output is thermal profiles vs. time and position. Finally, the code results were extended analytically to two dimensions

The following assumptions were used:

- water is used as a coolant
- all configurations use a microchannel heat exchanger with essentially the same design and characteristics (20 μm wide fins with a 10:1 etch depth ratio)
- the R&S with microchannel submounts configuration is allowed a higher effective heat transfer coefficient due to lateral spreading
- $\Delta T(T_{junction} - T_{water}) = 50\ ^{o}C$
- the effective fill factor is defined as diode cavity length (L) / laser bar spacing (pitch)

Four geometry's were considered. The first one is a planar monolithic configuration used in this program. The other three are R&S configurations with different pitches, the last one with individual microchannel submounts under every laser bar. Each pump geometry (layers and thickness') are further summarized in Figure 2.2.1.1.

The key result is that the monolithic configuration offers significant thermal advantages for duty cycles above 3% for both 200 μs and 1 ms long pulses. A very good thermal conductor such as Cu is needed for optimum transient performance, and the penetration depth into the Cu has to match the thickness of the Cu for optimum pulsed performance. A good match between the two exists for the 400 μm pitch R&S configuration which performs very well up to 3% duty cycles. The R&S with microchannel submounts configuration was designed primarily for CW operation (bars are mounted directly on Si), and so its thermal performance varies little with duty cycle, and it performs poorly under low duty cycle operation. The monolithic configuration, in spite of assuming lower wallplug efficiency, is overall superior over most of the duty cycle range and for different pulse widths, because its design minimizes the thermal path to the heat exchanger. From a thermal point of view, the monolithic approach is highly

desirable because it provides best performance over widest range of operating conditions.

GEOMETRY	CAVITY LENGTH (um)	PITCH (um)	EFFECTIVE FILL FACTOR	LAYER	THICKNESS (um)
1. MONOLITHIC SEA	500	1	1	GaAs GaAlAs In Cu In Si Si fins	100 2 4 700 4 50 200
2. RACK AND STACK (400 um PITCH)	750	400	1.88	GaAs GaAlAs In CuW BeO In Cu Si Si	100 2 4 200x1670 250 4 1000 50 200
3. RACK AND STACK (800 um PITCH)	750	800	0.94	GaAs GaAlAs In CuW Cu BeO In Cu Si Si	100 2 4 250x1670 400 250 4 1000 50 200
4. RACK AND STACK WITH MICRO-CHANNEL SUBMOUNTS	350	1,800	0.19	GaAs GaAlAs In Si GLASS+Si	100 2 4 50 1600

Figure 2.2.1.1 Pump Geometry Dimensions

2.2.2 Solid-State Laser Subsystem

TRW performed a set of trades to establish a solid state laser design that reduces risk and optimizes the performance of the microlaser array. The following is a brief discussion of the selection rationale and how they impact the laser design.

TRW selected Nd:YVO_4 as the baseline solid state material for integration in a microlaser array. This material has properties which make it uniquely suitable for Q-switched operation.

Nd:YVO_4 is a solid state material that has the highest known Nd:emission cross-section (2.7 x that for Nd:YAG[2]) and thus provides the maximum gain for a given inversion density. The high gain and emission cross-section (low saturation fluence) make it ideal for Q-switched operation. The introduction of Q-switching elements in the laser cavity typically results in significant loss and the high gains are essential for efficient extraction. The low saturation fluence reduces the risk of optical damage particularly in the case of the microlaser array where the ultrashort cavity length results in very short, high peak power pulses. In addition, the absorption coefficient of 1% doped Nd:YVO_4 is approximately 30 cm^{-1} which is comparable to high concentration stoichiometric materials. This allows the use of thin crystals (< 1 mm), which simultaneously provide high absorption efficiency and single longitudinal mode operation.

Yb:YAG was considered but ruled out for short pulse application because of its low emission cross section. Yb:YAG does, however, have several important advantages for CW operation. It is a quasi-three level system that is pumped at 0.95 μm which makes it an ideal candidate for surface emitting arrays. Since GaAs is transparent to the 0.95 μm wavelength, the diode array can be fabricated without etching the channels in the substrate through which the diode light exits. Furthermore, the microlenses can be etched directly on the substrate eliminating the lens assembly step. In addition, because of the very small quantum defect in Yb:YAG, it has a value which is on the order of 0.1[3]. Thus very little heat is produced in the material during the lasing process. It has a very long fluorescence lifetime of 1 ms at low doping levels and can be doped at concentrations up to 20% where the lifetime is only reduced to 500 μs. This long fluorescence lifetime partially compensates for the low emission cross-section which is 1.8×10^{-20} (1/15 that of Nd:YAG) and produces moderate small signal gains under long pulse or CW conditions. Yb:YAG also has a very broad

absorption spectrum, which significantly reduces the need for diode temperature control. The peak absorption coefficient at 20% doping levels is on the order of 18 cm^{-1}, which is adequate to provide efficient absorption in a crystal thin enough to provide single longitudinal mode operation.

The low emission crossection (high saturation fluence) makes Q-switched operation in Yb:YAG inefficient at high repetition rates (storage times << 1 msec) and susceptible to optical damage at low repetition rates (storage times 500 μsec.

Other materials considered included stoichiometric materials such as LNP[3] and LNA[2] which have high absorption, but they typically have products that are less than that of Nd:YVO_4 and Yb:YAG. Other well established materials such as Nd:YAG or Nd:YLF typically cannot provide high efficiency and single mode operation simultaneously, unless multiple stacks are used, which significantly complicates the laser design.

Mode control is achieved by insuring that the laser cavity mode spacing is larger than the laser gain bandwidth. This technique has been one of the key advantages of microlaser arrays and can be achieved simultaneously with high absorption efficiency, provided the material selected has very high absorption coefficient, such as in the case of Nd:YVO_4. Injection seeding and intracavity etalons are other common techniques used for mode control, but they represent a higher level of complexity.

The Q-switching for this program was done using a passive saturable absorber. The intent was to develop an understanding of the Q-switching physics in relation to an array of emitters before developing an active Q-switch approach.

2.3 Design Analyses and Performance Projections

2.3.1 Diode Array Subsystem

The baseline SEA point design is compatible with both wafer scale manufacturing and large scale assembly. The subarray consists of closely packed broad area single quantum well (SQW) graded-index separate confinement heterostructure (GRIN SCH) lasers connected in parallel in a 0.5 cm^2 area. The light exits through openings etched in the GaAs substrate and between Cu electrodes. The TRW baseline design for the CW diode laser array has an active area of 0.6 x 0.9 cm^2. It consists of 108 emitters, with cavity lengths of 1000 μm, 500 μm separation between emitters, and stripe widths of

100 μm. Efficiency is maximized for current levels of > 5* I_{th}, and outcoupling facet reflectivities of <10%. The TRW design is based on an output power density of > 100 W/cm^2, a power conversion efficiency η_C of > 0.4, and a power dissipation of < 200 W/cm^2. The latter is well within the microchannel heat exchanger capabilities. Modeling and design of the TRW microchannel has been published in the literature· In order to minimize ohmic losses a top current-spreading electrode of > 10 μm thick is required.

The principal requirements on array performance are lasing wavelength, spectral width and chirp, efficiency, output power, and thermal control.

Wavelength. The requisite center wavelength for pumping Nd:YVO_4 is 809 ± 2.5 nm and is achieved by varying the thickness of the quantum well and content of aluminum in the well.

Wavelength Bandwidth. Two sources contribute to the spread: fabrication process nonuniformity, and time-dependent wavelength chirp. MOCVD growth provides precise control of both aluminum content and layer thickness across large wafers, and excellent repeatability from wafer to wafer. Planar heat sinking insures maximum temperature uniformity across large areas.

The time-dependent wavelength chirp is associated with temperature rise (between 2.5 Å/°C to 3 Å/°C) during the pulse duration. The chirp is minimized by high efficiency operation and rapid heat removal. For sufficiently short pulses, the chirp is proportional to the square root of the pulse length. Our analysis indicated that 90% of the output power falls within a ~ 4 nm bandwidth, and was validated experimentally at operating levels two times threshold for 200 μs long pulses. The epi-down, planar heat sinking configuration insured efficient heat removal, minimizing chirp.

Efficiency and Peak Power. The efficiency and peak power depend on the efficiency of the single laser, engineering architecture of the whole subarray (electrode thickness required to minimize ohmic loss and electrical drive nonuniformities), materials and methods used for device fabrication, assembly, and packaging, and the efficiency of heat extraction techniques. The material we used was characterized by very low threshold current densities (200 to 300 A/cm^2 for a single well), and high differential efficiencies (80%).

2.3.2 Solid-State Laser Subsystem

The use of microlenses to collimate the fast axis of the diodes provides a new dimension in microlaser design flexibility. By minimizing the pump beam divergence in the solid state medium and reducing the pumped volume, the laser gain is increased by as much as an order of magnitude. This improves the extraction efficiency and facilitates Q-switching which typically introduces moderate amounts of loss and requires high gains. The design of the solid state laser is a relatively simple one which exploits this advantage and demonstrates integration of the microlaser array to a surface emitting diode array. Optical efficiencies greater than 20% can be achieved with wafers that are less than 500 μm thick. Simultaneously, maximum round trip gains on the order of 2.5 and 0.25 can be obtained in $Nd:YVO_4$.

$Nd:YVO_4$ has an emission bandwidth of approximately 7 Å[4] and single longitudinal mode operation requires a crystal that is less than 420 μm thick. The projected Q-switched optical efficiency of such a crystal is approximately 18% with a 1% doped crystal. This efficiency is based on a measured absorption coefficient of 30 cm^{-1} [4,5]. At slightly higher doping levels (1.5%), the efficiency increases to 22%. In long pulse mode (free running), the projected optical efficiency could exceed 30% and as with any diode pumped laser, the Q-switched optical efficiency improves as the pump pulse length becomes short compared to the medium lifetime. Thus, at 100 kHz rep-rates (10 μs integration time), the efficiency should approach that for long pulse operation. Because of the very high gains projected, the optimum outcoupler reflectance predicted by a Rigrod analysis is on the order of 60 -70%. 95% outcoupling efficiency was used to in the experiments to allow higher threshold devices to lase, and thus have as many elements lase as was possible.

Q-switching of the microlaser arrays provides the high peak powers required to improve signal to noise in many applications, as well as the opportunity to use nonlinear optics to obtain wavelength agility. The short cavity lasers provide very narrow pulses as demonstrated in the literature[3]. A model developed here predicts a primary pulse with a roughly 0.5 ns FWHM duration followed by several smaller secondary pulses. The secondary pulses are the result of the Q-switching time (1/e time of 0.5 ns), which is fast for most typical lasers, but is relatively slow for a microlaser.

Frequency doubling of the Q-switched laser would be achieved by using an intracavity KTP doubler. With a one way intracavity energy on the order of 20

μJ, a pulse duration on the order of 1 ns and a spot diameter of 100 μm, the intracavity intensity is approximately 250 MW/cm^2. Our calculations indicate that single pass conversion efficiencies in the range of 10 to 30% can be achieved in crystals that are 0.5 to 1 mm thick. Thus if the intracavity losses are on the order of 10%, a 0.5 mm crystal would yield 50% conversion efficiency. Higher efficiencies could be achieved with thicker crystals.

2.3.3 Thermal Analysis

The thermal issues are divided into those relating to heat deposited in the solid state laser crystal and those relating to direct diode heating. The big thermal advantage of the present surface emitting array approach is that the diode heat is in more intimate contact with the heat exchanger than with other approaches. The laser crystals in our design also have excellent thermal performance.

Each diode stripe produces 0.5 W optical output, and with a conservative 20% efficiency assumed, requires 2 W of thermal dissipation. The diode stripes are 1000 um long on 1000 um centers, and 100 um wide on 500 um centers. Thus, the local peak heat flux on a stripe is 2 kW/cm^2, while the area averaged heat flux is 400 W/cm^2.

The diode array layers below the heat source (active layer) are: 1.5 um of GaAlAs, 5 um of In solder, 1 mm copper, 0.25 um In-Sn solder, and then the heat exchanger. The microchannel heat exchanger, developed at TRW and has a thermal resistance as low as 0.015 C/W/cm^2, depending on the fin spacing selected.

Several different thermal analyses were performed for the diode heat removal: 1) two-dimensional steady-state conduction including effects of the many individual layers and lateral thermal spreading, 2) one-dimensional transient conduction including the many layers, and 3) two-dimensional transient conduction including only the heat source and the copper layer. The transient analyses show that the diode junction thermal spikes will be at most (for the 1 ms pulses) 5.1°C, which is only a 1.5 nm chirp. These thermal spikes are so small, because of the close proximity of the copper layer, and because the 1 mm copper layer thickness exceeds the thermal diffusion depth (0.63 mm in 1 ms).

The steady state analysis shows that for the 10% duty cycle, the junction to coolant temperature difference will be only 7°C (1°C through the copper, 6°C in the jet impingement heat exchanger, and other layers negligible). For CW

operation, the junction to coolant temperature difference will be 17°C (10°C through the 1 mm copper, 1.3°C for lateral thermal spreading from the stripes, and 5.7°C in the microchannel heat exchanger).

The solid state laser crystal is designed to absorb >90% of the incident diode optical power. Of this absorbed power, 32% turns to heat due to the quantum defect in Nd:YVO_4. This internal heating corresponds to Q = 0.14 W per spot where Nd:YVO_4 operates at a duty cycle of 10%. The heat diffuses radially (laterally) in the crystal from the spot to where the it is bonded to the GaAs, and through the diode array structure to the heat exchanger.

From the standpoint of the laser performance, the primary concern is temperature variations in the crystal across the lasing aperture. For circular spots, this center-to-edge temperature difference is given by $\Delta T = Q/4\Delta Lk$, where k is the thermal conductivity, and L is the crystal thickness. For crystal thicknessí which are on the order of 0.5 mm, $\Delta T = 0.78°C$, independent of spot diameter. The amount of thermal lensing introduced by these temperature gradients corresponds to a focal length of 7.5 for Nd:YVO_4. These values are much larger than the crystal thickness and actually provide a benefit by stabilizing the laser cavity.

There are additional temperature drops in the laser crystal outside the lasing area and through the bonding layer. These correspond to a temperature drop of 4°C in Nd:YVO_4. There are another 1 or 2°C drops through the other layers down to the diode junction temperature. Temperature variations of this magnitude outside the lasing area have no impact on the laser performance.

2.4 Fiber Lens Design

The microlenses used to collimate the HPSEA output are self-aligned to the emitting aperture, and rest in grooves etched in the GaAs substrate. Figure 2.4.1 illustrates the degree of collimation achieved for fiber microlenses with varying radii. Our baseline design uses 125 μm radii of curvature to achieve optimum collimation.

2.5 Q- Switching

The TRW approach for Q-switching in this program uses a passive saturable absorber. The issues associated with passive Q-switching are that variations in pump power are likely to result in a randomly distributed pulse

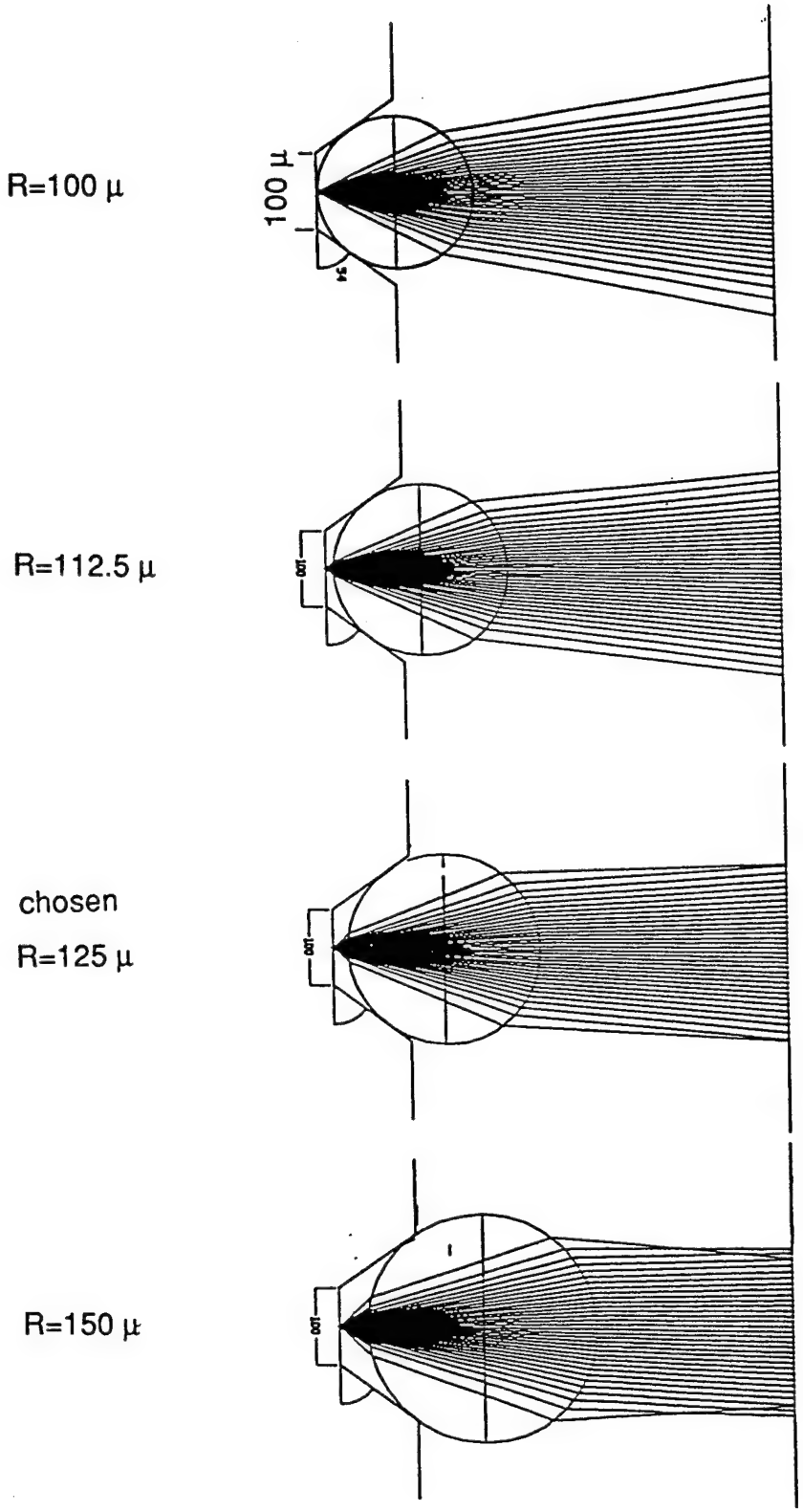

Figure 2.4.1 Diode light collimation achieved for fiber microlenses with varying radii.

envelope for an array of emitters, and that due to the long physical length of the Q-switch material (~ 1 cm), additional lenses are required in an external cavity configuration, to maintain a useful gain volume. To Q-switch an array of microlasers using this approach would require a very precise array of microlenses. Under this program an experimental validation of Q-switching was done using a single element.

A model was developed for Q-switching based on a one-dimensional, multilevel rate-equation model. It was anchored on a flashlamp pumped commercial Nd:YAG laser with good agreement.

3. FABRICATION

3.1 Pump Array Fabrication

This section summarizes the fabrication procedures that produced the SEAs for this program. This includes material growth, SEA device processing, and packaging and assembly of the microlaser arrays. The SEA configuration is illustrated in Figure 3.2.1 in the next section. The SEA dimensions were 0.8 cm x 1.1 cm, which included a 0.6 cm x 0.9 cm active area with a 1 mm rim surrounding it. The rim was used primarily to facilitate handling during the processing and packaging sequence.

Material Growth. To minimize costs, single quantum well graded index active regions material grown by MOCVD was obtained from several outside vendors. The epitaxially grown laser structure consisted of a 50 angstrom thick undoped GaAs active region, 1500 angstrom thick linearly graded (30% to 60% Al) undoped GaAlAs waveguide regions, 1.5 μm thick $Al_{0.5}Ga_{0.5}As$ cladding regions doped p and n type ($5x10^{17}$ cm^{-3}) with Zn and Si respectively, and a 0.25 μm thick Zn doped p+ cap layer ($1x10^{19}$ cm^{-3}).

SEA Device Processing. The processing sequence is outlined below

STEP #	PROCESS
1	Material test. A broad area laser is fabricated on a section of the wafer to test the wafer quality and material properties (threshold current, wavelength, efficiency, etc.)
2	Clean wafer. The wafer is cleaned using a standard RCA cleaning process.
3.	Stripe definition. The laser stripe is defined by lithography and wet chemical etching (H_2SO_4:H_2O_2:H_2O)
4	45 degree mirror etching. The pattern is defined lithographically, followed by ion milling at an angle to form the mirror, and removal of the remaining photoresist.
5	90 degree mirror etching. The pattern is defined lithographically, followed by reactive ion etching using $SiCl_4$ gas to form the mirror, and removal of the remaining photoresist. An SEM inspection step follows the etching of the two mirrors.
6	Si_3N_4 passivation. Si_3N_4 is deposited over the entire wafer surface using plasma enhanced chemical vapor deposition (PECVD).
7	Open contact regions. The ohmic contact areas are opened in the nitride by defining the stripe areas lithographically, followed by reactive ion etching of the nitride, and removal of the photoresist layer
8	p-metal liftoff. The p-metal is applied to the wafer by defining the stripe areas lithographically, followed by p-metal deposition (Ti/Pt/Au), and the liftoff of the photoresist. The remaining metal covers the laser stripes only.
9	HR coating. This is another lift-off process which covers the vertical laser mirrors with a layer of Ti/Au. The Ti/Au is applied to the wafer by defining the deposition areas lithographically, followed by metal deposition at an angle, and liftoff of the photoresist. The remaining metal covers the vertical mirrors only.
10	Polyimide deposition. Polyimide is deposited to fill in the mirror holes and planarize the wafer. The polyimide is then patterned using a photoresist cover, and is etched everywhere else. The photoresist cover is then removed, leaving just the Polyimide, which is then cured.
11	Lapping and polishing. The wafer is lapped down to 4 mils, and polished.
12	n-metal lift-off. The laser outcoupling mirrors are defined lithographically using a flip-chip infrared mask aligner. The holes in the substrate are positioned to match the 45^o mirrors on the epitaxial side. Following the lithography, n-metal (Ni/AuGe/Ni/Au) is evaporated on the n-side of the wafer.. The metal is then lifted off to allow openings for the outcoupling mirrors.

SEA Processing Steps

STEP #	PROCESS
13	Ohmic contact annealing. The ohmic metals are annealed in a forming gas environment.
14	Electrical screen tests. The IV characteristics of individual unit cells are evaluated.
15	p-metal overlay. A Ti/Pt/Au metal overlay is deposited on the p-side of the wafer.
16	Unit cell mounting. Individual unit cells are mounted on Cu bases using In solder
17	Window etch. The outcoupling mirrors are etched in the GaAs substrate material using a wet chemical etch (H_2O_2:NH_3 solution)
18	Pre-packaging. The unit cells are cleaned, I-V characteristics are re-measured, and are ready for packaging.

SEA Processing Steps (continued)

Highly precise and reproducible vertical and 45 degree micromirrors, and "through substrate" outcoupling mirrors, were critical to achieve efficient surface emitting devices. An ion-milling technique (angled milling through a photoresist mask was used to fabricate the 45^{o} micro-mirrors, and reactive ion etching (RIE) was used to fabricate the vertical micro-mirrors. The outcoupling mirrors were etched to within 2 μm of the active region by etching through approximately 100 μm of GaAs material using a wet chemical etch (H_2O_2:NH_3 20:1) which stops when it reaches a high Al content GaAlAs etch-stop layer. The surface smoothness of these mirrors matches that of the epitaxial growth. Atomic force microscopy measurements of ion-milled mirrors indicate RMS surface roughness of less than 19 nm over a 10 μm long measurement region (i.e. $\lambda/12$ inside the material).

3.2 Packaging Integration and Assembly.

After the SEA arrays were made, they were mounted with solder in an array package consisting of top and bottom Copper electrodes, separated by a ceramic spacer. The bottom electrode is soldered directly to a microchannel heat exchanger. Figure 3.2.1 shows a schematic diagram of this SEA package.

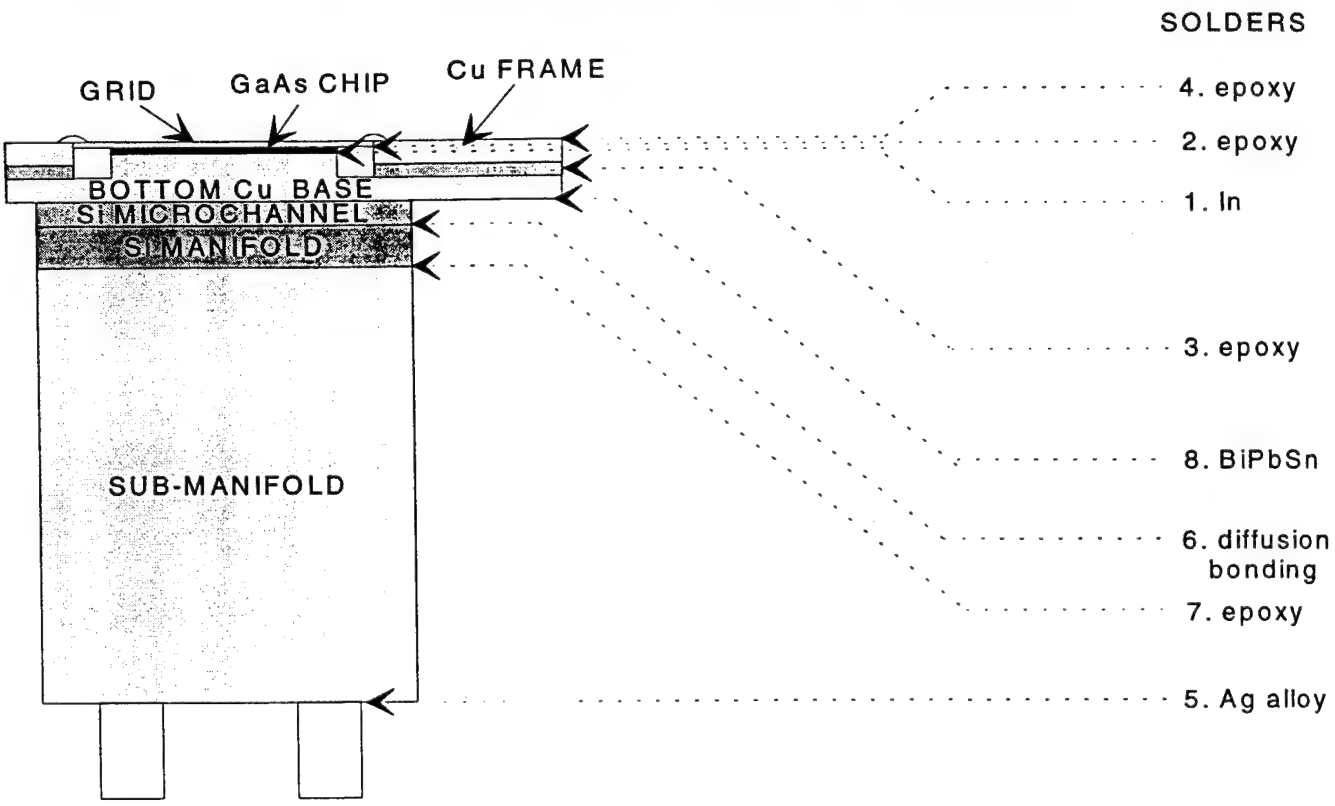

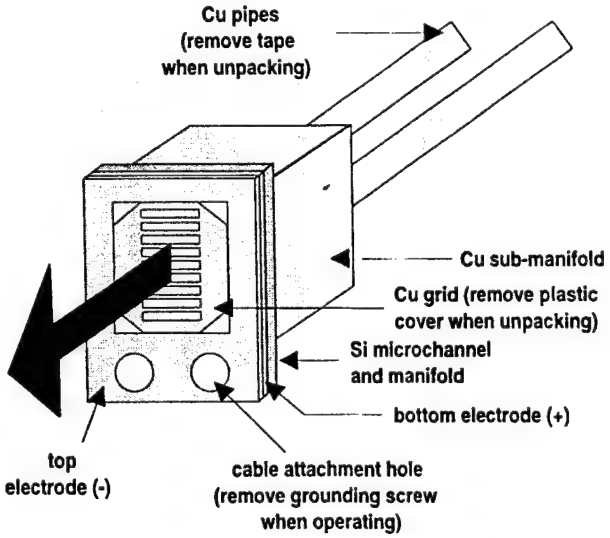

Figure 3.2.1 - Schematic Diagram of the SEA Package

The two key parts of the microchannel heat exchanger are the microchannel fin structure and the coolant distribution manifold. Both were fabricated by silicon etching technology from <111> orientation, high resistance silicon wafers polished on both sides. In the correct crystallographic orientation, Si has the extraordinary property of allowing KOH etching with a depth to width ratio of up to 100:1. The microchannels were etched in 10 mil thick silicon wafers, while the manifold was etched in 1 mm thick wafers. The fabrication procedure is outlined in Figure 3.2.2.

STEP #	PROCESS
1	Standard RCA silicon wafer cleaning procedure
2	Thermally grow Si_3N_4 in a low pressure CVD. A thickness of approximately 800 angstroms is deposited to create a resilient masking layer that will tolerate a long etching duration.
3	Photoresist deposition of mask
4	Etch pattern in Si_3N_4 using reactive ion etching, followed by removal of the photoresist.
5	Etch Si wafers with 44% KOH
6	Syrip Si_3N_4 using an HF acid etch.

Figure 3.2.2 Microchannel Fabrication Procedure

The manifold processing is the same as the microchannel process, except that the wafer is etched from both sides to produce open distribution channels and the coolant inlet and outlet passages. In etching the manifold, it is critical to achieve precise alignment of the microchannels with the correct crystallographic direction. Otherwise, lateral etching will not be suppressed, and the required high depth to width ratio will not be achieved. Therefore, a shallow preliminary etch of a "splay" pattern was done at the edge of the wafer. The splay pattern is an array of fine lines whose inclinations vary by 0.1 degrees. Microscopic examination of the etch results determined the correct alignment for the etch mask.

After etching of the microchannel and manifold were complete, they were diffusion bonded together. The steps are outlined in Figure 3.2.3.

STEP	PROCESS
1	Wafer preparation for bonding: Wafer scrubbing, RCA cleaning process, and rinse dry with a spinner-rinse machine, and dry with hot N_2 jets.
2	Contact: Bring top wafer (microchannel) and bottom wafer (manifold) into contact in an aligning fixture.
3	Inspection: Inspect in IR microscope to insure perfect wafer pattern match.
4	Annealing: Anneal wafers for 3 hours at 1100 °C.
5	Wafer sawing: Saw the heat exchanger modules from the bonded wafers.

Figure 3.2.3 Microchannel/Manifold Bonding Procedure

Microlens and Solid-State Laser Slab Integration Shown in Figure 3.2.4 is a cross section of the microlaser array after the fiber microlenses and Nd:YVO_4 solid state laser had been integrated with the packaged SEA.

Microlenses were aligned as follows:

STEP	PROCESS
1	Grooves matching the laser diode emitter spacing were etched in a GaAs substrate which served as an assembly registration/alignment fixture.
2	Fiber lenses were positioned in the grooves
3	The copper electrode (grid) was brought in close proximity to the alignment fixture, and the fibers were epoxied on the grid using a UV-curable epoxy. The end result was a rigid microlens array imbedded in the copper grid.
4	The grid/microlens array were epoxied to the GaAs substrate using electrically-conductive epoxy to complete the integration process.

After the microlenses were integrated with the SEA package, the Nd:YVO_4 slab was attached to the copper grid with Indium solder.

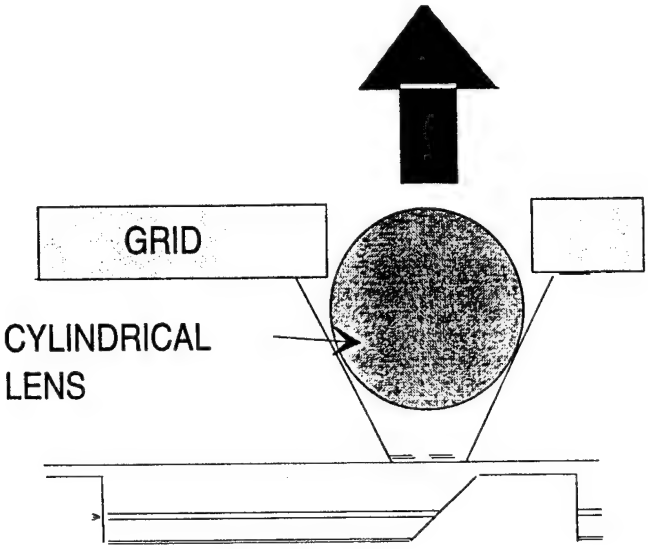

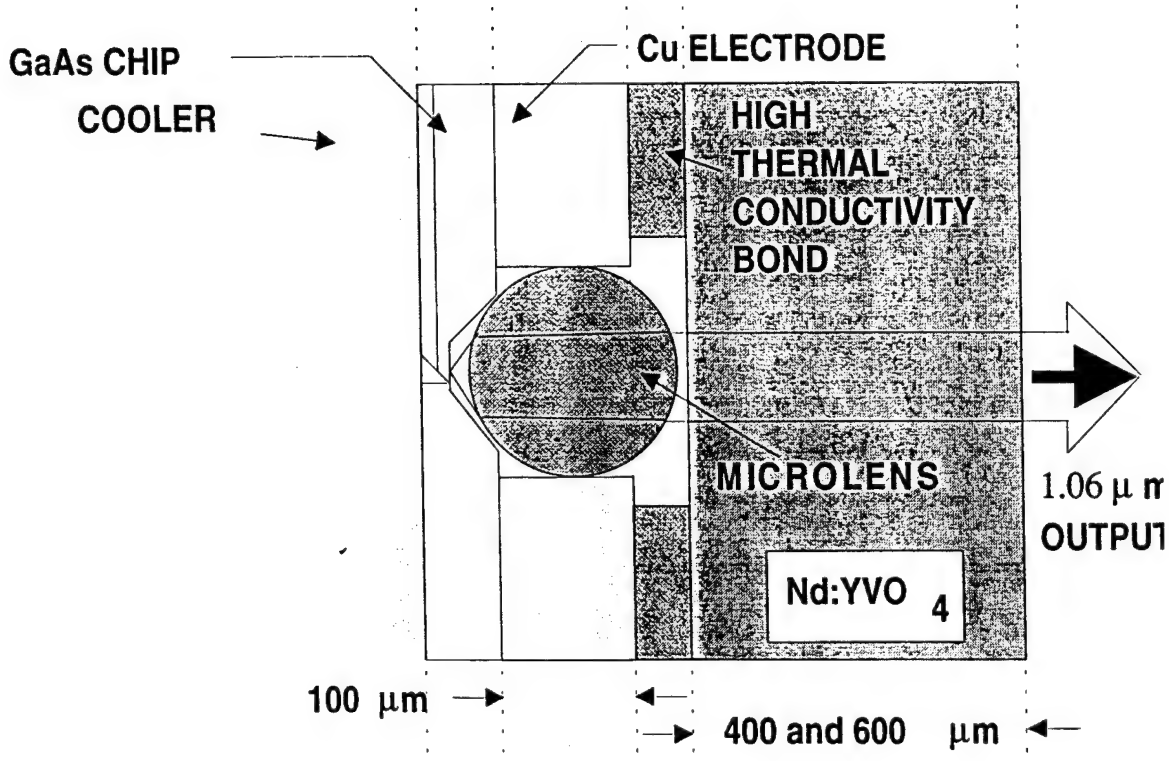

Figure 3.2.4 Microlaser array after microlens and Nd:YVO_4 Integration

4. TEST AND CHARACTERIZATION

4.1 Validation Experiments

4.1.1 Absorption

The material absorption was determined, before the chips were coated, using a CARY spectrum analyzer. The relevant geometry is shown in Figure 4.1.1.1. The results of those measurements are shown in Figure 4.1.1.2 and have the Fresnel losses, 21.3%, subtracted and only the region of interest is shown. Material from Litton and from Castech, China were measured with no noticeable difference in absorption noted. The material absorption was measured using both the a and c polarization.

4.1.2 Single Element Microlasers

4.1.2.1 Ti-Sapphire Pump

A series of experiments were performed with a tunable Ti:Sapphire laser to pump the Nd:YVO_4 to characterize the optical efficiency of the material in a controlled manner before performing the diode pumping experiments. In the first experiment an external outcoupler was used and the effects of varying cavity length were observed. The experimental geometry for that experiment is shown in Figure 4.1.2.1. A detail of the microlaser optics is shown on Figure 4.1.2.2. The output face of the Nd:YVO_4 was AR coated for this experiment. A mechanical optical chopper was placed in line with the CW Ti:Sapphire laser to produce 125 micro second pulses. A 50 cm focal length lens produced a spot size at the Nd:YVO_4 of 80 microns. The wavelength of the Ti:Sapphire laser was monitored with a wave meter. The cavity length could be controlled and the output power was measured as a function of the cavity length as shown in Figure 4.1.2.2. Also shown on this figure is a theoretical plot of gain vs. cavity length. This curve reflects the mode size variation with cavity length. As the cavity length increases the mode size decreases and the mode averaged gain increases. The oscillations in measured output power reflect the transmission characteristics of the etalon produced by the uncoated Nd:YVO_4 and the outcoupler.

In a second experiment the optical efficiency was determined when the Nd:YVO_4 was coated so that the chip length was the cavity length. The output face of the chip was coated as an outcoupler with 95% reflectivity. The results of that measurement is shown in Figure 4.1.2.3. The highest optical efficiency was measured in this configuration. Also shown in this figure is the single point

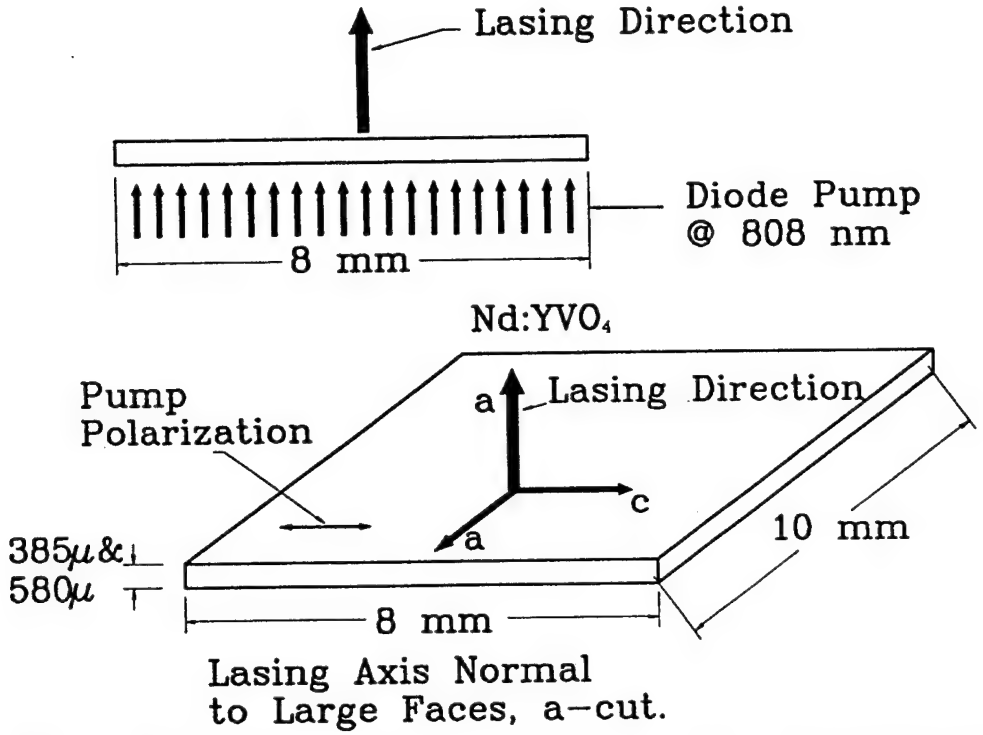

Figure 4.1.1.1 Relavent geometry for the absorption measurements of $Nd:YVO_4$

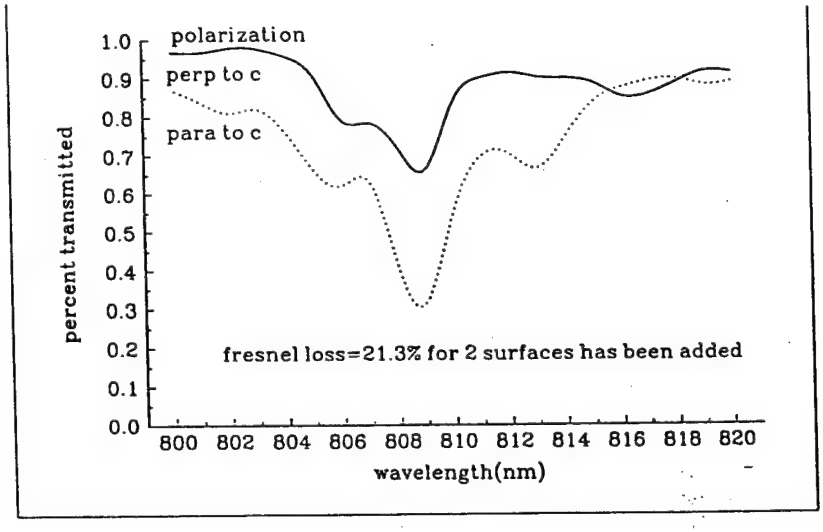

Figure 4.1.1.2 Absorption measurements of uncoated $Nd:YVO_4$

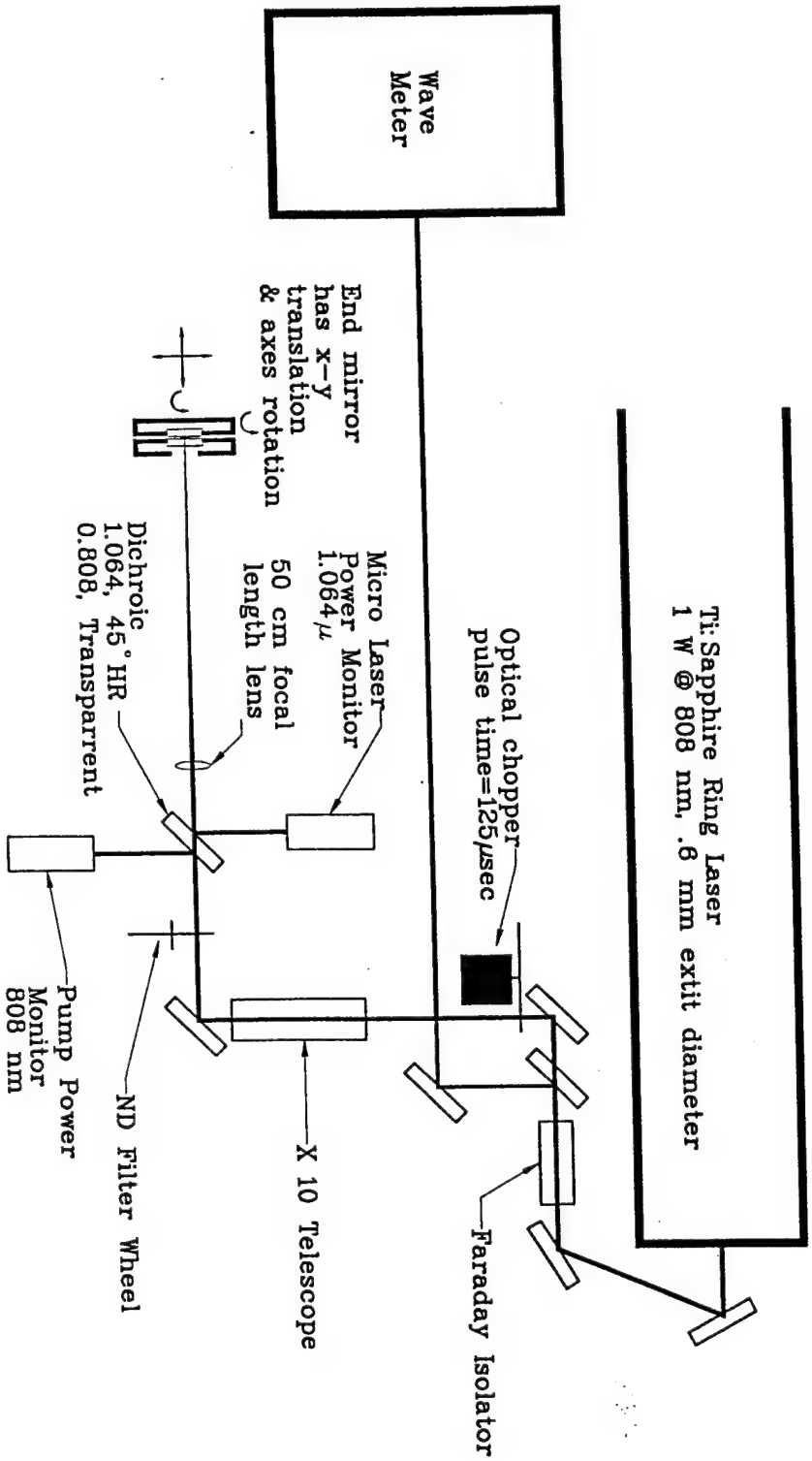

Figure 4.1.2.1 Ti:Sapphire pumping with variable cavity length. External Output mirror.

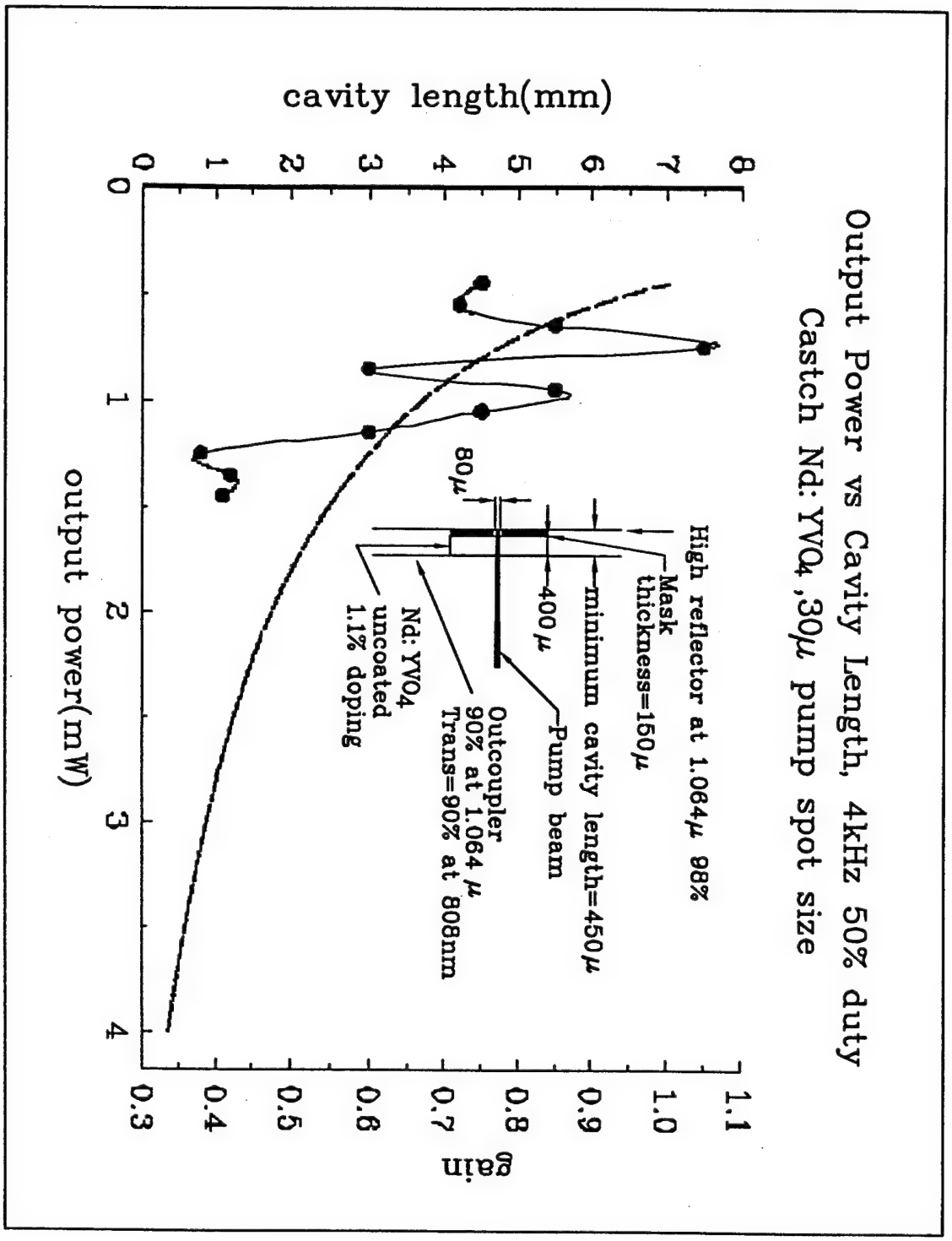

Figure 4.1.2.2 Detail of the chip geometry and the experimental results for Ti:Sapphire pumping of Nd:YVO_4 with variable cavity length. Theoretical curve shown. Oscillation due to etaloning.

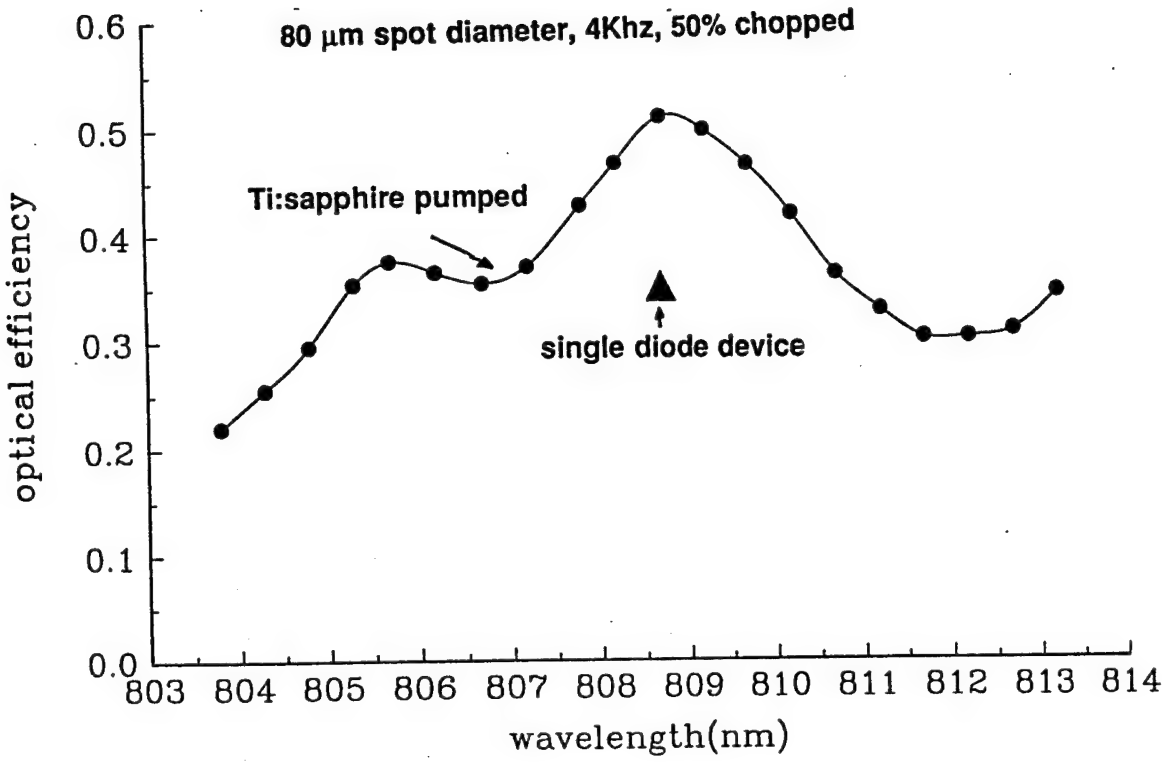

Figure 4.1.2.3 Optical efficiency measurements for Ti:Sapphire pumping of Nd:YVO_4 with outcoupler on the chip. Single point is the single diode pump result.

measurement for single diode pumping. Figure 4.1.2.4 shows excellent far field beam shape. The far field divergence was determined to be 3.5 mradians.

4.1.2.2 Laser Diode Pump

The Nd:YVO_4 was also pumped with a single diode device. The chip was coated as shown in Figure 4.1.1.2. Diode light was focused by a lens into a tight spot onto the Nd:YVO_4. The single diode device output was 1.0 W with an output at 1.064 μm of 350 mW for an optical efficiency of 35%. The output was also single longitudinal mode as expected due to the cavity configuration. The device was run CW. This compared favorably with the Ti:Sapphire results as shown in Figure 4.1.2.4. The efficiency was not as good as the Ti:Sapphire results because the diode light could not be focused as well as the Ti:Sapphire laser which has much smaller divergence than the diode laser.

4.1.3 Fiber Lenses

The fiber lenses proved to be simple to install and no alignment was necessary. The 250 micron diameter quartz fibers simply dropped into the channels. Collimating was verified by observing the collimated light on a white card placed above the array at 45 degrees. All the light from the 108 emitters could be observed this way and the collimation of each could be verified. Each of the 9 sprays of light corresponded to each of the 9 columns of diode emitters. The recorded light pattern did not increase in size which indicated that the light is collimated. The sprays of light were not vertical which indicated the fibers were offset slightly from the emitters. This is due to the minor inaccuracies in the channel manufacturing. This small angle does not effect the performance of the micro lasers but does cause a minor inaccuracy in the exact array position of the microlasers. One can also see that the sprays are not all identical. This is due to the fact that the diode array elements are not identical, some are not emitting at all.

4.1.4 Q-Switching

Q-switching was demonstrated using the saturable absorber, Cr^{4+}:YAG, and Ti:Sapphire pumped Nd:YO_4. The experimental configuration for this test is shown in Figure 4.1.4.1. The lens was used in the cavity to make the mode size as small as possible. The gain in the resonator is averaged over the mode area, so that even though the pumped volume was very small, 50-80 micron diameter,

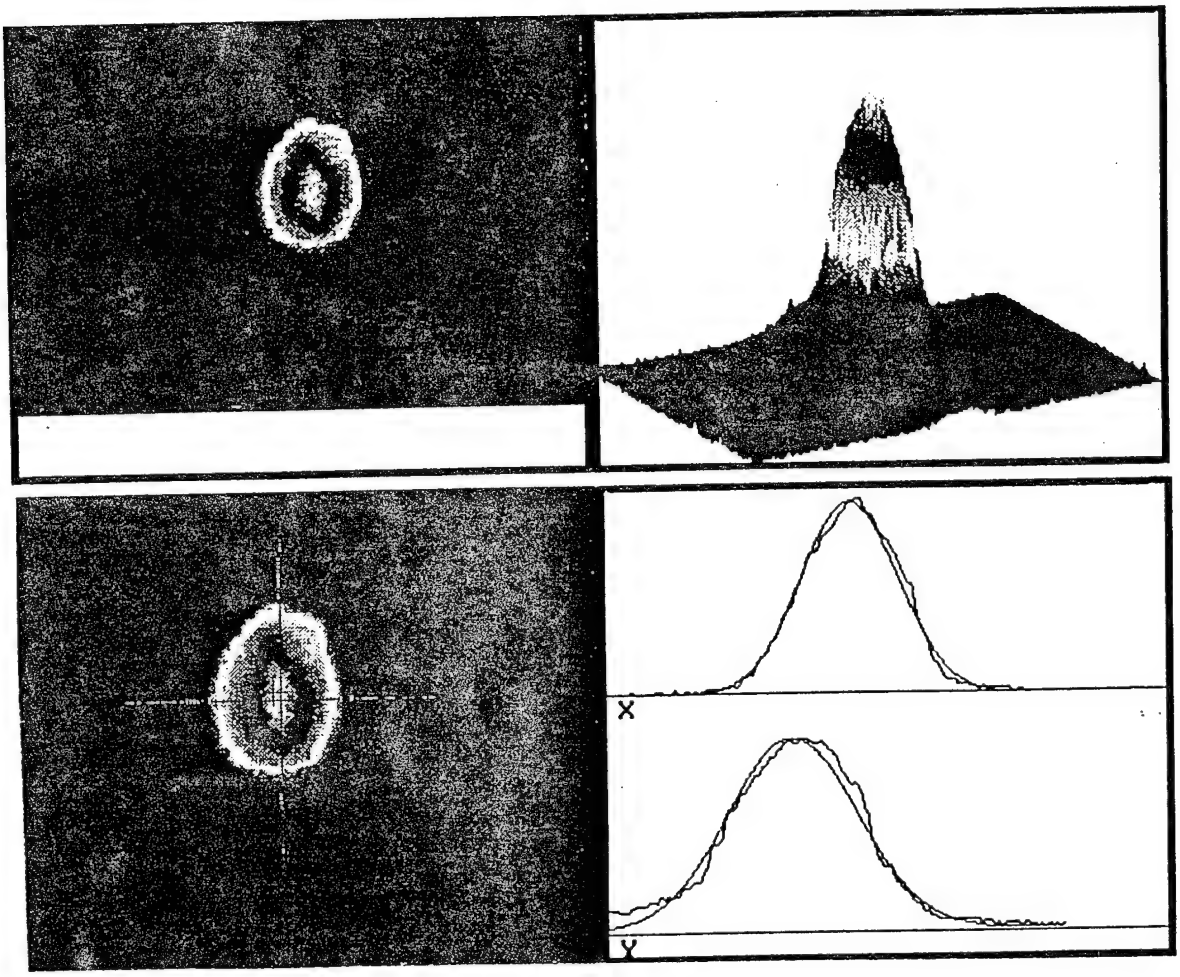

Figure 4.1.2.4 Far Field of Ti:Sapphire Pumped Nd:YVO_4 with Outcoupler on Chip.

the gain would be too small to lase without mode control. Even with the lens, the pulse energy was small and the pulse duration was long. Figure 4.1.4.1 shows a picture of the pulse train characteristic of a saturable absorber Q-switch and a detail of an individual pulse. The optical efficiency was 25% and the pulse width was 150 ns.

4.2 Array Measurements

The diode array was first coupled to the vanidate in an open cavity with an outcoupler that was separate from the vanidate. Later the vanidate was coated so that no external optics were required, all the cavity coating were on the vanidate itself.

The initial coating on the vanidate had one surface with an AR coating at the pump wavelength and HR coating at the lasing wavelength. The opposite surface had an HR coating at the pump wavelength and an AR coating at the lasing wavelength. The coatings for the pump wavelength allowed the pump to transmit on the incoming face and reflect on the opposite face so that the pump could double pass the vanidate for efficient absorption. The lasing took place between the HR surface and an external outcoupler.

When the laser array was operated in this way, only portions of the array lased at any one time. As the outcoupler alignment was varied, different portions would lase. The entire surface of the vanidate which had the HR coating could not be made parallel to the outcoupler all at once due to the surface irregularities. Either the initial surface shape or more probably, the thermally modified surface shape, was not flat.

The validate was recoated as shown in Figure 4.1.1.4 so that the surfaces on the vanidate would form the entire laser cavity. The thermal lensing would ensure that each element would find its own lasing axis. The surface that was AR coated at the lasing wavelength was recoated for 95% reflectance. When operated in this way, each element in the array that could lase would lase.

The wavelength variation of the pump array was first measured and is shown in Figure 4.2.1. Shown as an inset in this figure is the measured absorption spectra taken with the Ti:Sapphire laser. The 2D array had a broader spectra than desired and explains to some extent the results that follow. The spectrum shown is for one particular operating diode coolant temperature which

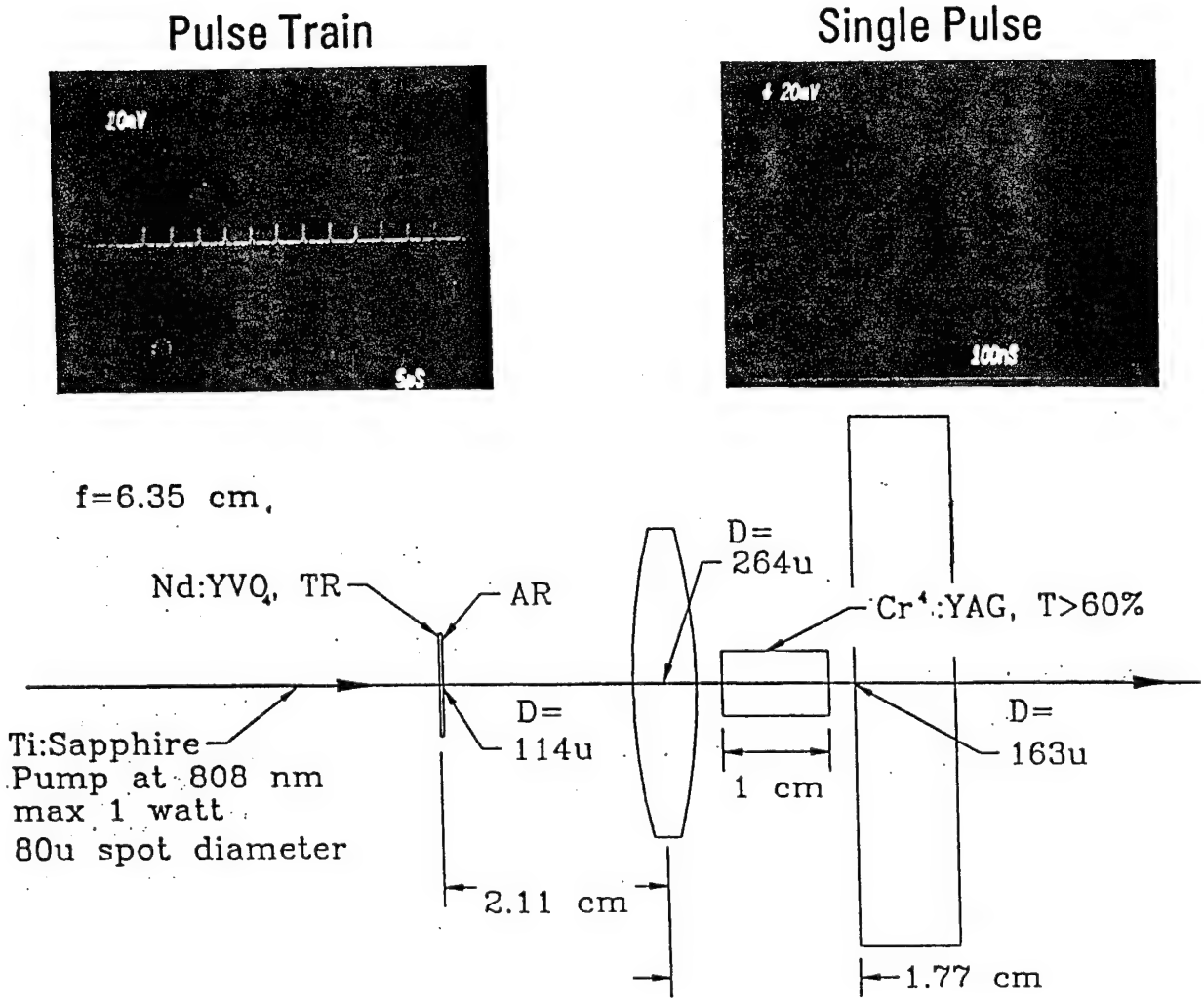

Figure 4.1.4.1 The experimental configuration for the saturable absorber Q-switch test and the saturable Q-switch pulses.

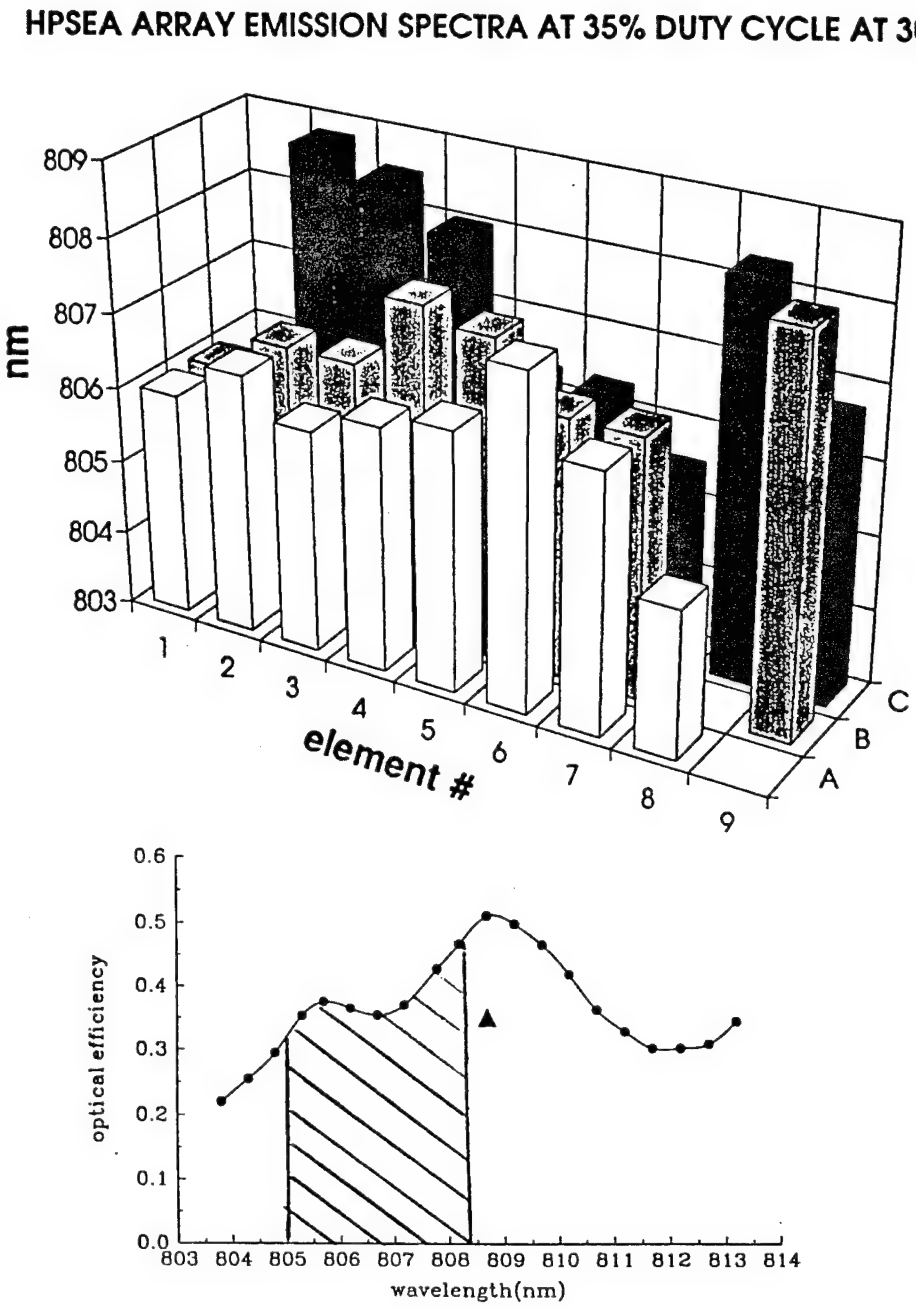

Figure 4.2.1 The Measured Wavelength Variation of the HPSEA Device. Inset is the Measured Absorption Spectra of the Nd:YVO_4.

corresponds to an optimum in 1 micron lasing output power from the entire 2D array. As the coolant temperature varied the distribution would generally follow. The required temperature was high enough (30 C) to significantly shorten the lifetime of the diode array.

The output of the 1 micron vanidate laser is shown in Figure 4.2.2 and a histogram of the lasing intensities is shown in Figure 4.2.3. A majority of the non lasing element count was due to dead elements in the pump array. A smaller portion was due to pump elements that were operating but at a wavelength that was too far out of band so that sufficient energy could not be stored in the vanidate for lasing. The slope efficiency of the entire array is shown in Figure 4.2.4.

Single mode operation of the 2D array was confirmed by a measurement of the output spectrum of the array. Figure 4.2.5 shows the spectrum under a few operating conditions. Each element in the array operated in only one longitudinal mode but each element had a different single mode wavelength due to the cavity length variations that had to do not only with the variation in static thickness of the vanidate but more importantly with the variation in thermally induce lengths. The spectrum shown indicated that those variations are of the order of $\pm$20%. Transverse modes were not seen and were not expected. The gain volume was smaller than the fundamental transverse mode size. The gain is averaged over the mode size and thus the smaller the mode size the greater the gain. Higher order transverse modes, having larger mode size, had smaller gain and were thus not seen.

5. CONCLUSION

This program demonstrated the technical feasibility of 2D micro laser arrays which can be able to produce 2 watts of output power at 1 micron. The assembly and operation of the microlaser array are simple and require no complicated alignment procedures. The material choice of vanidate proved to be an excellent one. Vanidate efficiently absorbs the 808 nm radiation when it is oriented properly with respect to the polarization of the diodes. The material demonstrated an optical efficiency of 50% when pumped at the peak of its absorption. 70% of the elements in the 2D array lased for an output of 350 mW at 35% duty cycle.

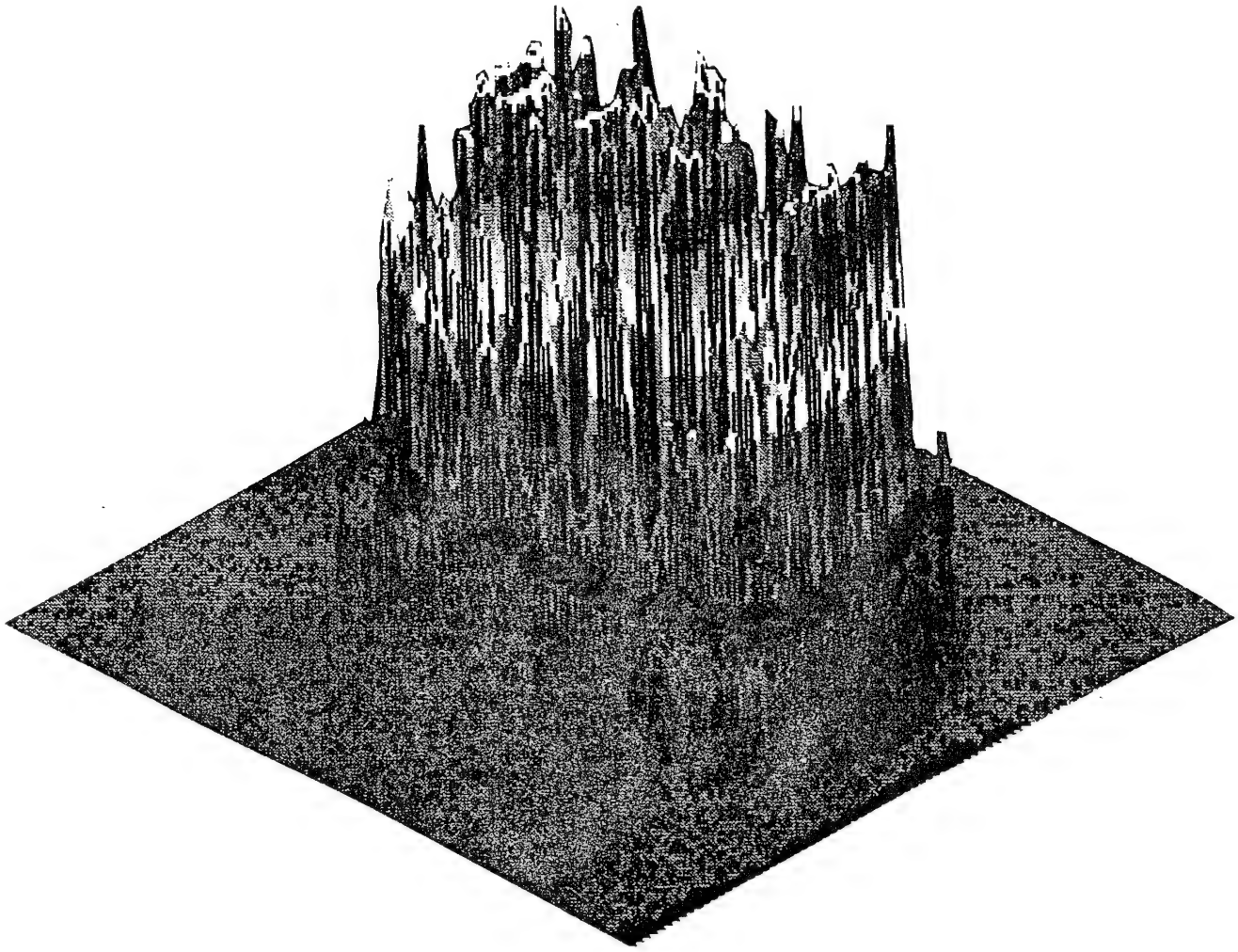

Figure 4.2.2 Intensity Profile of the Output of the 2D Micro Laser Array.

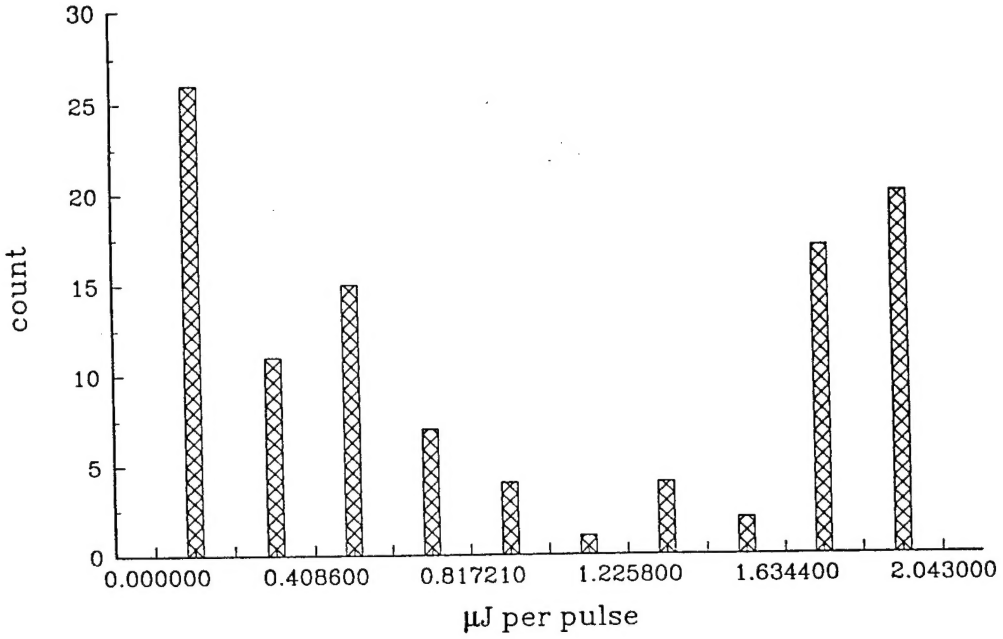

Figure 4.2.3 Histogram of the Output of the 2D Micro Laser Array. >70% of the Array was lasing. 12% optical efficiency for those devices at 2 μJ.

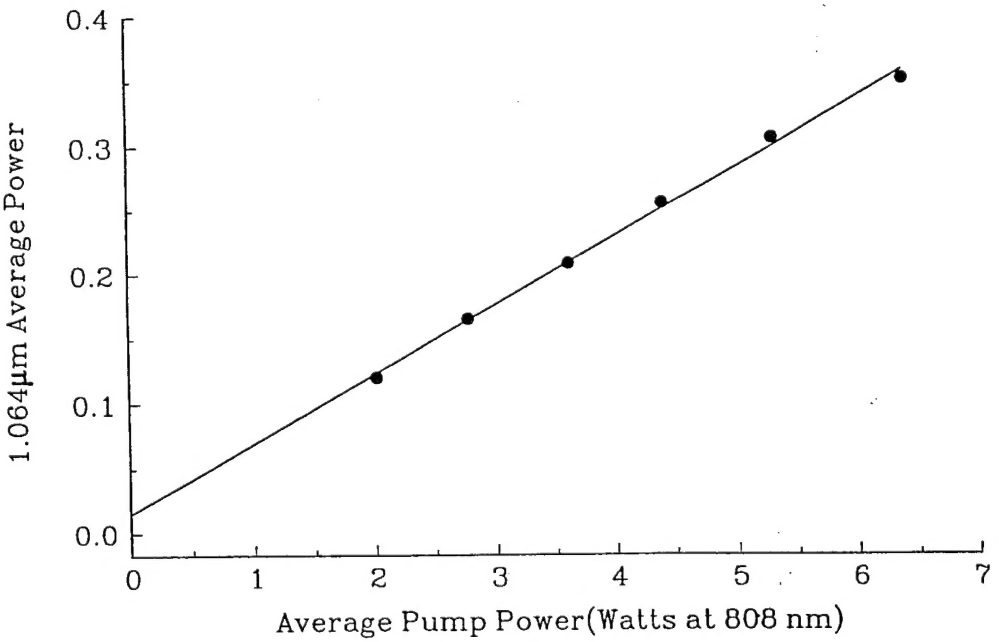

Figure 4.2.4 Slope Efficiency of the 2D Micro Laser Array is 5.8%.

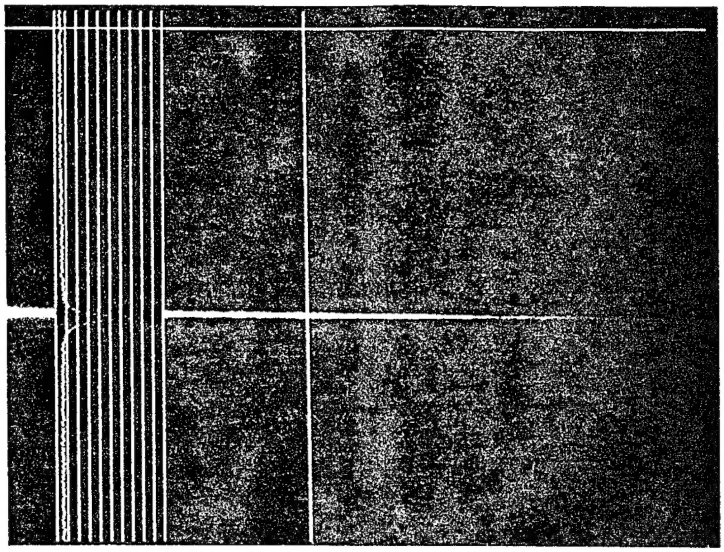

Single element spectrum

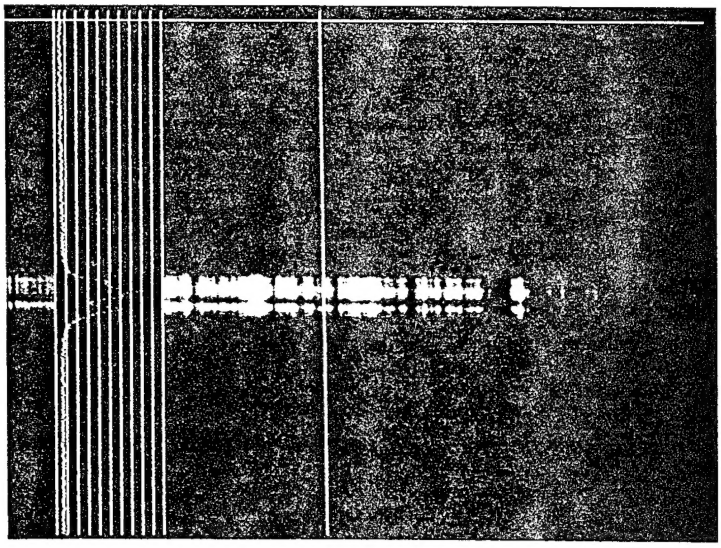

Entire array spectrum, $\Delta\nu$=43 GHz

Figure 4.2.5 Single Longidutinal Mode Spectrum of the 2D Micro Laser Array. Variations in the Spectrum Indicate Individual Cavity Lenght Variations within the Array.

6. REFERENCES

1. J. R. Leger, "Lateral mode control of an AlGaAs laser array in a Talbot cavity", Appl. Phys. Lett. **55** (4) 334 (1989).

2. "Performance comparisons of diode pumped neodymium laser materials", OSA Proceedings on Tunable Solid State Lasers, Edited by Michael L. Shand and Hans P. Jenssen, May 1-3 1989.

3. J. J. Zayhowski, J. Ochoa, and A. Mooridian, "Gain-switched pulsed operation of microchip lasers", Optics Letters, Vol. 14, No. 23, 1989.

4. L. DeShazer, private communication.

5. Takunori Taira Akira Mukai, Yukihiro Nozawa, and Takao Kobaysahi, "Single-mode oscillation of laser-diode-pumped Nd:YVO_4 microchip lasers", Optics Letters, Vol. 16, No. 24, 1991.

6. R. H. Tan, R. J. Simes, and L. A. Coldren, "Electroabsorptive Fabry-Perot Reflection Modulators with Asymmetric Mirror", IEEE Photonics Technology Letters, Vol. 1, No. 9, 1989.

7. R. H. Tan, R. J. Simes, and L. A. Coldren, "Extremely Low-Voltage Fabry-Perot Reflection Modulators" IEEE Photonics Technology Letters, Vol. 2, No. 2, 1990.

8. B. Pezeshki, D. Thomas, and J. S. Harris, Jr., "Large Reflectivity Modulation Using InGaAs-GaAs", IEEE Photonics Technology Letters, Vol. 2, No. 11, 1990.

9. J. Z. Wilcox, S. S. Ou, J. J. Yang, M. Jansen and G. L. Peterson, "Dependence of External Differential Efficiency on Laser Length and Reflectivities on Multiple Quantum Well Lasers", Appl. Phys. Lett., **55**, 825 (1989).

10. J. Z. Wilcox, S. S. Ou, J. J. Yang, M. Jansen and G. L. Peterson, "Dependence of Emission Wavelength on Cavity Length and Facet Reflectivities in Multiple Quantum Well Semiconductor Lasers", Appl. Phys. Lett., **54**, 2174 (1989).

11. J. Z. Wilcox, S. S. Ou, J. J. Yang, M. Jansen and D. Schecter, "Gain Dependence of The Threshold Characteristic Temperature in Multiple Quantum Well Lasers", Appl. Phys. Lett., **53**, 2272 (1988).

12. J. Z. Wilcox, G. L. Peterson, S. S. Ou, J. J. Yang, M. Jansen and D. Schechter, "Gain and Threshold Current Dependence for Multiple Quantum Well Lasers", Journal of Applied Physics, 64, 6564, (1988).

13. J. Z. Wilcox, G. L. Peterson, S. S. Ou, J. J. Yang, and M. Jansen, "Length Dependence of Threshold Current in Multiple Quantum Well Lasers", Electronics Letter, 24, 1218, (1988).
14. S. S. Ou, J. J. Yang, J. Z. Wilcox, and M. Jansen, "Characterization of Double Quantum Well GaAs/AlGaAs Diode Lasers", Electronics Letters 24, 952, (1988)
15. S. S. Ou, J. J. Yang, M. Jansen, M. Sargant, L. J. Mawst and J. Z. Wilcox, "High Performance Surface-Emitting Lasers with Intracavity 45° Micromirror", Appl. Phys. Lett., 58,16,1991.
16. . S. S. Ou, M. Jansen, J. J. Yang, M. Sargant, "High Power CW Operation of GaAs/GaAlAs Surface-emitting Lasers Mounted in the Junction-Up Configuration", Appl. Phys. Lett., 59,1037,(1991).
17. S. S. Ou, M. Jansen, J. J. Yang, L. J. Mawst and T. J. Roth, "High Power CW Operation of GaAs/GaAs Surface-emitting Lasers with 45° Intracavity Micromirrors, Appl. Phys. Lett., 59, 2085,(1991).
18. M. Jansen, J. J. Yang, S. S. Ou, M. Sargant, L. Mawst, J. Rozenbergs, J. Wilcox and D. Botez, "Monolithic Two-Dimensional Surface-emitting Laser Diode Arrays Mounted in the Junction-down Configuration, Appl. Phys. Lett., 59, 2663, 1991)